Schlieren imaging and pulsed detonation engine testing of ignition by a nanosecond repetitively pulsed discharge

Joseph K. Lefkowitz [a],*, Peng Guo [a], Timothy Ombrello [b], Sang Hee Won [a], Christopher A. Stevens [c], John L. Hoke [c], Frederick Schauer [b], Yiguang Ju [a]

[a] Deparment of Mechanical and Aerospace Engineering, Princeton University, NJ 08544, USA
[b] Aerospace Systems Directorate, Wright-Patterson AFB, OH 45433, USA
[c] Innovative Scientific Solutions Inc., Dayton, OH 45459, USA

ABSTRACT

A nanosecond repetitively pulsed (NRP) discharge in the spark regime has been investigated as to its effectiveness in reducing ignition time, both in a flow tube and a pulsed detonation engine (PDE). The flame-development time for methane–air mixtures in the flow tube is found to be a function of the total ignition energy and the pulse repetition frequency. Schlieren imaging revealed that at low pulse-repetition frequency (0–5 kHz), ignition kernels formed by the discharge are each transported away from the discharge gap before the following pulse arrives. At higher pulse-repetition frequencies ($\geqslant 10$ kHz), multiple pulses are all coupled into a single ignition kernel, thus the resulting ignition kernel size and the total energy deposition into the kernel are increased, resulting in a faster transition into a self-propagating flame. Imaging of the NRP discharge in air revealed that at high pulse frequencies (>10 kHz) and peak pulse amplitude (>9 kV), the plasma emission is not quenched in-between pulses, resulting in a building up of heat and radicals in the center of the ignition kernel. Optical emission spectra revealed the presence of electronically excited N_2, O, and N, as well as O^+ and N^+, during and between the discharge pulses. Numerical modeling of the plasma indicated that reactions of excited species mainly lead to the production of O atoms and the increase of gas temperature, which shortens induction chemistry timescales, and thus reduces the flame-development time through both kinetic and thermal mechanisms. Ignition of aviation gasoline–air mixtures by NRP discharge in a PDE also demonstrated a noticeable reduction in ignition time as compared to an automotive aftermarket multiple capacitive-discharge ignition system.

© 2015 The Combustion Institute. Published by Elsevier Inc. All rights reserved.

1. Introduction

The development of reliable ignition sources for combustion systems which operate near the conventional flammability limits and within restricted residence times is a major bottleneck for technologies such as lean burning internal combustion engines, gas turbine engines (relight and afterburner ignition), scramjets, and pulsed detonation engines (PDEs) [1,2]. The ignition kernel development time, typically taking about half of the overall combustion time in spark ignition engines, is controlled by the mixture reactivity, temperature, pressure, and ignition energy source [3–5]. In real engines, heterogeneous fuel/air mixtures, non-zero bulk flow velocities, and local turbulent fluctuations all affect the required energy for successful ignition kernel generation [6,7].

Because of these variations in required energy, the minimum ignition energy (MIE) for fuel–air mixtures in demanding applications can be significantly greater than the MIE determined in quiescent environments. In addition, for applications such as PDEs, decreasing the ignition time directly affects the overall thrust of the engine. Consequently, how to provide this energy most effectively is a topic of study as old as the internal combustion engine itself.

In the work of Maly [3], the optimal ignition device is described as one that (a) deposits the energy needed for ignition in the shortest possible time period, (b) creates an expanding plasma volume with the highest possible surface velocity, (c) reaches the largest possible plasma radius, (d) does not supply additional energy after the flame has propagated beyond the plasma radius, and (e) only deposits energy into a narrow spherical shell propagating away from the electrodes. To fulfill these basic criteria, short duration (10–100 ns) plasma discharges have been suggested as a method to reduce ignition times while increasing energy deposition

efficiency as compared to capacitor discharge ignition systems (CDI, typically 0.1–0.3 ms spark duration) or transistorized coil ignition systems (TCI, typically 1–5 ms duration) [3,8]. The effectiveness of this discharge type is due to the deposition of most of the discharge energy into the breakdown phase of the gas discharge.

In order to form a gas discharge, a large energy input is required to ionize the initially neutral gas molecules and induce an electron avalanche, which in turn dissociates, excites, and ionizes the molecules and atoms in the discharge gap. After the initial breakdown phase, which occurs on the order of a few nanoseconds at atmospheric pressure, the discharge can develop into a longer lifetime glow, arc, or streamer discharge. The breakdown phase has a high peak current (on the order of 100 A) as compared to arc (order of 1–10 A) and glow (order of 0.1–1 A) discharges, and thus has a faster energy deposition than these other plasma discharge types [3,8]. While all atmospheric pressure discharges must be initialized by the breakdown phase, the proportion of energy into each phase can be controlled by the peak initial voltage and duration of the discharge. After the breakdown stage, a steep temperature and active species concentration gradient is set up around the interelectrode region, which propagates outwards from this region into the unburned mixture. Additional energy deposition after the breakdown into the following arc or glow stages primarily serves to heat the gas between the electrodes, and is largely ineffective from an ignition perspective if the initial breakdown has enough energy to ignite the mixture. However, if the initial breakdown does not supply enough energy to bring the ignition kernel to the critical radius and temperature for transition to a freely propagating flame [5,9], or if the initial propagation rate is sufficiently slow, then there is time to add energy into the ignition kernel and reduce its development time. This can be accomplished by increasing the duration of the discharge pulse, or by depositing multiple pulses into a single ignition kernel.

To take advantage of the efficient energy deposition in the breakdown phase, nanosecond duration discharges have recently been investigated [1,2,10,11]. Notably, single pulse ignition using a transient plasma igniter (TPI) has been shown to reduce ignition time compared to conventional spark discharges in both engines and quiescent environments [12–16]. The faster ignition times in methane–air and ethylene–air mixtures were attributed to the multiple simultaneous streamer type discharge channels heating a larger gas volume than the conventional spark discharge. Also, a contribution from kinetic enhancement via reactions of excited species and radicals created during the breakdown due to the high reduced electric field (*E/N*) was reported. It was also found that the ignition time was independent of the duration of the discharge in the range of 10–50 ns, and was only significantly affected by the pulse rise rate and the peak *E/N* (i.e., peak voltage for constant discharge gap and gas density). Pancheshnyi et al. [17] explored ignition behavior using a nanosecond repetitively pulsed (NRP) plasma in quiescent propane–air mixtures using a pin-to-pin configuration. Each pulse was below the breakdown threshold for the gas mixture, but it was found that multiple pulses caused significant pre-ionization and eventually breakdown, leading to temperatures in excess of 3000 K and significant dissociation and ionization. The ignition time could be decreased with the application of additional discharge pulses beyond the minimum amount necessary to ignite the mixture if the MIE for the mixture was greater than the per pulse energy of the discharge. This was attributed to a building up of neutral radicals in the ignition kernel before the flame propagated away from the discharge region.

The purpose of the present study is to extend the understanding of NRP discharges as an ignition source to flowing environments and practical aerospace fuels, as well as to explore the inter-pulse coupling effect and the fuel kinetic effects contributing to changes in the ignition time. For this purpose, a 12 ns duration plasma discharge with a repetition frequency of up to 40 kHz is used with a pin-to-pin electrode configuration for ignition in two experimental platforms. First, the dynamics of kernel development and subsequent flame propagation for ethylene-air and methane–air mixtures in a turbulent flow field are observed in a flow tube using schlieren imaging. Second, NRP discharge ignition is tested in a PDE and compared to conventional capacitor discharge ignition (CDI) in ethylene–air and aviation gasoline (avgas)–air mixtures. Testing of NRP discharges in the glow and corona regimes in PDE engines has been previously shown to reduce ignition time compared to conventional ignition [16,18–20]. This study aims to extend the fundamental understanding of the observed ignition enhancement by determining the controlling parameters leading to reduced ignition times using NRP discharges in the spark regime.

2. Experimental and numerical methods

2.1. Plasma igniter

Both a NRP discharge and a multiple spark discharge (MSD, P/N 62152) system were tested parametrically in this study, as outlined in Table 1. The NRP power supply (FID GmbH FPG 30-50MC4) produces peak pulse amplitudes of 22 kV, pulse duration of 12 ns FWHM, and pulse repetition frequencies of up to 40 kHz. Three values were used for the peak open-circuit voltage in the present experiments: 9 kV, 15 kV, and 22 kV, while the frequency is varied in the range of 0.869–40 kHz and the number of pulses is varied from 2 to 200. The MSD igniter is an aftermarket automotive CDI device, which produces a series of sparks (generally 3 for the current set of experiments) at a fixed pulse repetition frequency of 0.869 kHz. The peak voltage of the MSD igniter was measured to be 6.5 kV, and after breakdown produced a peak current of 15 A for a power pulse of approximately 1 µs followed by a current pulse continuing for 50 µs thereafter [16]. This type of plasma can be characterized as an arc discharge. The MSD power supply provides between 105 and 115 mJ, however, values between 5 and 10 mJ were measured in these experiments due to the poor efficiency of arc discharge energy deposition [3,8]. The same nonresistive spark plug (Autolite Racing AR3911) and cable were used in all experiments. The ground strap of the spark plug was removed and replaced with a sharpened steel electrode, and the center electrode was sharpened to a point to produce a pin-to-pin configuration. The spark gap was fixed at 1.4 mm, which was found to be the maximum gap distance permissible to ensure the discharge occurred only between the two electrodes. The voltage and current traces were measured using a LeCroy high voltage

Table 1
Discharge parameters for both MSD and NRP igniters. Parameters in MSD are fixed.

Igniter	Average energy/pulse (mJ)	Pulse duration (ns)	Pulse frequency (kHz)	Number of pulses	Open-circuit voltage (kV)	Max current (A)
NRP	0.8, 1.9, 3.2	12	0.869–40	2–200	9, 15, 22	20–50
MSD	5.7	≈1000	0.869	3	6.5	15

probe (PPE20KV) and a Pearson Coil (Model 6585), respectively, on the 3 m cable from the power supply to the spark plug. In the case of the NRP discharge, a 300 Ω resistor was connected in parallel with the power supply to supply a constant load and damp reflections in the voltage pulse.

Plasma energy measurements were made following the method outlined by Pancheshnyi et al. [17]. The displacement current is computed as $I_{Disp} = C\frac{dV(t)}{dt}$, where the measured capacitance (C) is 18 pF. The conduction current is the difference between the measured current and the displacement current. The total energy was computed by integrating power over the initial pulse using $P(t) = V(t) * I_{Cond}(t)$ and $E = \int P(t)dt$. Analogous to the results of Pancheshnyi et al. [17], the peak current and voltage were not constant, but rather the voltage was higher in the first few pulses, while the current was lower in the following pulses. This corresponds to the pre-breakdown and streamer to spark transition, which increases the conductivity of the gas until all pulses are in the spark regime [17,21,22]. The first pulse was never sufficient to cause gas breakdown, but did create significant pre-ionization for breakdown to occur on the second pulse for all of the pulse amplitudes tested. After the first three pulses, the voltage and current waveforms of the discharge are repeated for all subsequent pulses. In addition, pulse frequency had only a small effect on the pulse energy. The accuracy and uncertainty of the measurements of ignition energy deposition are highly sensitive to the bandwidths of both the voltage probe (100 MHz, 3.5 ns rise time) and the Pearson Coil (200 MHz, 1.5 ns rise time), which are close to the ≈5 ns rise time of the NRP discharge pulse. This causes relatively large uncertainties considering that the entire waveform is needed to calculate the energy, not just the peak voltage or current. We estimate the total uncertainty of the NRP discharge energy measurements to be 50% of the total energy. This was due to the time resolution of the measurement devices, interference from reflected pulses which could not be eliminated in this system, pulse-to-pulse variation in energy deposition, changes in electrode geometry due to wear, and unaccounted parasitic losses. Energy measurements of NRP discharges using the measurement devices herein, as well as with similar devices, are discussed in further detail in Refs. [17,21–23].

NRP discharges in the pin-to-pin configuration have been shown to operate in three regimes: corona, glow, and spark. Pai et al. [21] have outlined the conditions in which these discharges exist in terms of applied voltage, pulse frequency, inter-electrode distance, and ambient gas temperature. The different regimes are characterized by increasing discharge current and emission intensity in the visible range, particularly from electronically excited and ionized nitrogen (N_2 C–B (0,0) and N_2^+ (B–X) (0,0) transitions). Pai et al. reported that only corona and spark discharges existed in their system below 700 K gas temperature at a 5 mm inter-electrode distance, 30 kHz pulse repetition frequency, and 1–10 kV max voltage. Based on these findings, and visible observation, the discharge used in this study is in the spark regime, as the lowest voltage used is 9 kV, the inter-electrode gap is 1.4 mm, and the ambient temperature is at maximum 400 K, precluding the possibility of corona or glow discharges. In spark discharges, rapid temperature increase in the narrow discharge channel leads to a fast pressure rise, and a shock wave propagates outwardly from the discharge after the initial breakdown pulse. The presence of this shock wave is apparent in the Schlieren imaging, which is further evidence of the spark regime.

2.2. Pulsed detonation engine

The PDE facility is described in detail in Refs. [16,24,25]. The engine consists of four detonation tubes, two of which were fired

in this study, one as the experimental platform and the other one as a dummy ballast tube. The system is built on a General Motors Quad-4 Dual Overhead Cam (DOHC) 4-cylinder engine head. In place of the cylinder and piston assemblies, steel detonation tubes 185 cm in length and 5.08 cm in diameter are bolted to the engine head. The experiment tube is fitted with a Shchelkin-like spiral to enhance turbulence generation and facilitate the deflagration-to-detonation transition (DDT), the length of which was 91.4 cm for ethylene experiments and 121.9 cm for avgas experiments.

The PDE works on a three-phase (fill, fire, and purge) cycle. The fill phase of the cycle consists of filling the detonation tube with premixed flammable gases through the intake valves of the engine head, after which the intake valves are closed and the fire phase begins. The fire phase is subdivided into three steps: first, a user determined "ignition delay" is applied to allow pressure transients to dissipate. Second is the "ignition time," initiated by the triggering of the igniter, and consisting of the time for the ignition kernel to develop into a self-propagating flame and undergo DDT. Third is detonation wave propagation, which produces a rapid pressure rise, accelerating the burned gas through the detonation tube, and producing thrust. The purge phase follows, in which a half-tube fill of air is pumped through the exhaust valves of the engine to purge the burned gas, and the cycle is then repeated. All tests were conducted at an engine cycle rate of 10 Hz.

The PDE diagnostic system consists of a dynamic pressure transducer in the engine head and nine ion probes located at equal intervals of 15.24 cm along the detonation tube, starting 25.72 cm from the engine head. The ignition time is determined when the signal from the pressure transducer reaches a slope of 5 V/s. The position and speed of the deflagration or detonation wave is monitored by the ion probes. When two consecutive wave speed measurements first result in the same measured value, the wave speed is determined to be the C–J velocity. To determine the DDT distance, the wave speed is linearly interpolated between the measurements just before and after the C–J velocity is reached. The DDT time is determined by calculating the time when the wave reaches the DDT distance.

2.3. Flame-development visualization platform

For the flame-development visualization experiments, the detonation tube is replaced by a steel tube 261.6 cm in length and fitted with a 91.4 cm long, 5.08 cm × 5.08 cm square test section with polycarbonate walls, as depicted in Fig. 1 [26]. The Schlieren imaging setup consists of an LED light source, collimating mirrors, a knife edge, and a Phantom v711 high-frame-rate Complementary Metal-Oxide Semiconductor (CMOS) camera. The light emitted from the LED source is collimated by one of the mirrors and sent through the polycarbonate walls of the schlieren test section. A mirror setup identical to the collimating mirrors focuses the light onto the CMOS chip of the camera, with part of the light blocked by the knife edge. Images were collected beginning just prior to the ignition event and continued until the combustion wave had fully propagated out of the view of the camera. The frame rate was fixed at 100 kfps with 2 μs exposure time.

To process these images, the frames before the ignition event were averaged to provide a background image which all subsequent images were divided by. For the images provided in the following section, a color look-up table was applied for increased color contrast and hence better visual identification of the flame front. A flame tracking program developed in MATLAB® using its built-in edge finding function, and employing the Canny method [27], was used to monitor the evolution of the flame front by finding the local maxima in pixel intensity gradients and tracking the evolution of these maxima throughout the images of each ignition
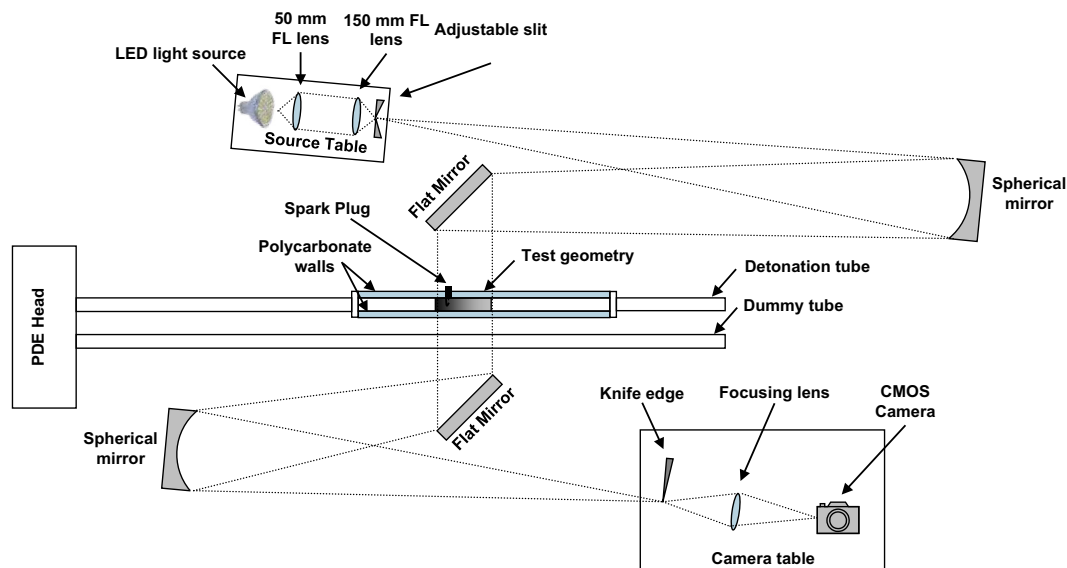
Fig. 1. Schematic of the flame-development visualization experiment [26].

event [28]. Due to the turbulent flow environment, the ignition kernel was far from symmetric and the flame front was not always sharp in the images, thus the results from the edge tracking program cannot accurately be used to measure the flame speed as is done in laminar spherically propagating flames [9,28]. Instead, the leftmost and rightmost edges are tracked, and the difference in pixels between them is referred to as the area of the kernel. The rightmost pixel in the ignition kernel, before it develops into a self-propagating flame, is used to determine the bulk gas velocity. The average initial velocity was found to be 10 ± 2.5 m/s in all flow visualization experiments. Because these experiments were performed in a modified PDE, the flow velocity is changing throughout the cycle, and is also subject to cycle-to-cycle variations typical of engine experiments. Thus, the exact velocity throughout the flame-development process cannot be accurately determined.

High-frame-rate imaging and optical emission spectrometry (OES) measurements of the NRP discharge were also performed in quiescent laboratory air. The high-frame-rate images were performed at 390 kfps with 2 μs exposure time using a Phantom v711 CMOS camera. The camera was focused in a region of ≈ 1 cm^2 containing the electrode gap and surrounding air. The emission intensity ranging from 400 to 950 nm was extracted as a function of time to determine the lifetime of the plasma discharge. To quantify the emission intensity, the average pixel value in the image domain was calculated for each image. As the onset of emission generally saturates the CMOS sensor for the 2 μs exposure time used, the peak intensity cannot be extracted accurately. To truly measure peak emission intensity, a shorter exposure time or a neutral density filter could be used to bring down the total photon count on the CMOS sensor. However, the aim of the present measurement is to monitor the inter-pulse emission, which is significantly less intense than the peak emission, and thus no effort was made to decrease the light intensity. The optical emission spectroscopy measurements were conducted using an Ocean Optics USB2000+ spectrometer which operates in the range of 190–874 nm with an optical resolution of ≈ 1.4 nm FWHM, and has been calibrated for a flat response across the operating wavelength range. The light is collected through an optical fiber focused on the center of the electrode gap, and averaged in time over the entire NRP discharge burst.

2.4. Numerical modeling

To approximate the plasma processes in NRP discharges, ZDPlasKin [29], a plasma chemistry reaction solver incorporating BOLSIG+ [30] for calculation of electron-collision reactions, and the SENKIN package of CHEMKIN II [31] are coupled together to efficiently model species evolution in 0-dimensional plasma-assisted combustion (PAC). Gas heating during the plasma is calculated in the method of Flitti and Pancheshnyi [32], which accounts for energy coupled into the translational temperature of electrons and of the bulk gas separately. The simplified methane–air plasma model of Aleksandrov et al. [33] is used as the basis for the plasma chemistry, and ethylene reactions from Lefkowitz et al. [34] are added to complete the model for ethylene–air. The plasma species considered follows the example of Aleksandrov et al. [33], and includes $N_2(A^3\Sigma_u^+)$; $N_2(B^3\Pi_g)$, $N_2(B'^3\Sigma_u^-)$, $N_2(W^3\Delta_u)$ (all grouped as $N_2(B)$); $N_2(a'^1\Pi_g)$, $N_2(a'^1\Sigma_u^-)$, $N_2(w^1\Delta_u)$ (all grouped as $N_2(a')$); $N_2(C^3\Pi_u)$; N_2^+; $O_2(c^1\Sigma_u^-)$, $O_2(C^3\Delta_u)$, $O_2(A^3\Sigma_u^+)$ (all grouped as $O_2(4.5$ eV$)$); $O_2(a^1\Delta_g)$; $O_2(b^1\Sigma_g^+)$; O_2^+; CH_4^+; CH_3^+; $C_2H_4^+$; $C_2H_3^+$; $C_2H_2^+$. The electron-collision cross-sections for O_2, N_2, and CH_4 are downloaded from the LXCat online database [35–37], and cross-sections for C_2H_4 are computed in the method described by Janev and Reiter [38]. Quenching reactions from the plasma model are added to the combustion chemistry model USC-Mech II [39] to create a simplified reaction scheme for methane–air and ethylene–air PAC at elevated temperatures (>800 K) to operate during the inter-pulse time. The aim of this model is not to include every relevant species in the plasma, but only the ones responsible for principal generation of radicals and heat release. Because the Poisson equation for the electric field distribution is not solved, and thus charge separation and sheath formation are not considered, the reduced electric field (E/N) cannot be explicitly calculated from the measured applied voltage. Thus, an estimated E/N value of 320 Td was assumed in order to mimic the experimental results for emission intensity. Specifically, a large enough value of E/N such that the radical concentration did not fully decay between pulses for the 40 kHz case was selected. The degree of radical production was manipulated via the duration of the plasma pulse in the model. Note that spark discharges can only truly be modeled by a multi-dimensional

scheme; however, this 0-dimensional model is found to be sufficient to give an estimate of which radicals are created by the plasma and the lifetimes of these radicals.

3. Results and discussion

3.1. Flame-development visualization

To gain an understanding of the effects of peak voltage, pulse repetition frequency, and the number of pulses in a burst on flame-development dynamics, each of these parameters were varied independently in both the flow visualization and PDE testing platforms. The ignition visualization experiments were carried out for stoichiometric methane–air and ethylene–air mixtures. Two timescales were identified for comparison of ignition events: the flame-development time, which represents the time it takes for the kernel to reach 10% of the total area of the observation domain, and the rapid burning time, which is the time it takes for the flame to go from 10% to 90% of the observation domain [4]. In the ethylene–air experiments, no significant improvement of flame-development time was found; however, for methane–air mixtures the flame-development time was found to be a function of total ignition energy and pulse frequency. The rapid burning time was found to be insensitive to the ignition device or discharge parameters for both fuels.

In Fig. 2, images of the ignition event at 4 ms after the initial discharge in a stoichiometric methane–air mixture visually represent the effects of pulse energy and pulse number on the flame-development time. The pulse repetition frequency was fixed at 40 kHz for all images. For fixed energy per pulse, the growth rate of the ignition kernel increases with the number of pulses up to 50 pulses, which corresponds to 1.25 ms after the initial pulse. Further increases in pulse number produces negligible reduction in the flame-development time since the kernel surface has already moved away from the inter-electrode region and is transitioning into a self-propagating flame. For fixed number of pulses, there is little difference between the 1.9 mJ/pulse and 3.2 mJ/pulse conditions; however, the 0.8 mJ/pulse condition exhibits a significantly slower flame-development process, indicating some fundamental change in the discharge properties if the pulse energy is too low. The MSD ignition is comparable to the three pulse NRP experiments at 1.9 and 3.2 mJ/pulse, but is significantly slower than the 20 pulse NRP experiments. The flame-development time as a function of total ignition energy for all methane–air visualization experiments is summarized in Fig. 3. The total energy (average
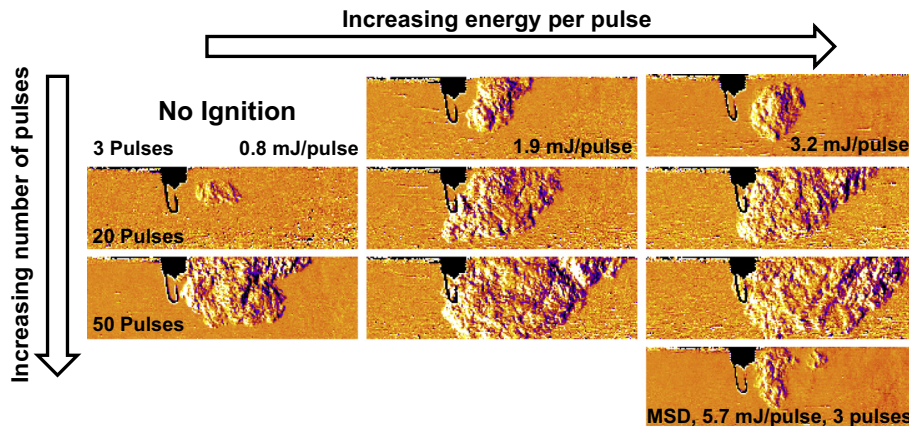
Fig. 3. Flame-development time extracted from schlieren imaging of stoichiometric methane–air ignition events for varying total energy deposition and pulse frequency.

energy per pulse multiplied by number of pulses) of the discharge has a strong effect on the flame-development time, as evidenced by the best fit to the high frequency data. In addition, at pulse repetition frequencies below 10 kHz the flame-development time is significantly increased. A closer look at low and high frequency ignition events reveals why this is the case.

Figure 4 compares two ignition events, both with 16 mJ total energy deposition (5 pulses at 3.2 mJ/pulse), but one with a pulse repetition frequency of 2 kHz (one pulse every 0.5 ms, total time of 2.5 ms) and the other at 40 kHz (one pulse every 0.025 ms, total time of 0.125 ms). The 2 kHz condition is displayed in the left panels, with each image corresponding to a new voltage pulse for the first three images. With a time interval of 0.5 ms between pulses, the bulk gas velocity of 10 ± 2.5 m/s transports each kernel 4–6 mm from the inter-electrode region before the next voltage pulse arrives, which is far enough to prevent additional energy from the discharge to enter into the ignition kernel. Every subsequent pulse creates a new ignition kernel, which combines with previous ignition kernels downstream of the inter-electrode region, in this case forming two large distinct flame regions visible by 2 ms after the initial discharge. By 4 ms, the two large kernels have separated further, and by 6 ms both kernels have begun to transition into self propagating flames. At even lower frequencies, the kernels would never interact downstream of the electrodes,

Fig. 2. Schlieren images of stoichiometric methane–air ignition 4 ms after the initial discharge pulse for both NRP and MSD ignition systems. NRP pulse frequency = 40 kHz. Gas flow = 10 ± 2.5 m/s from left to right.
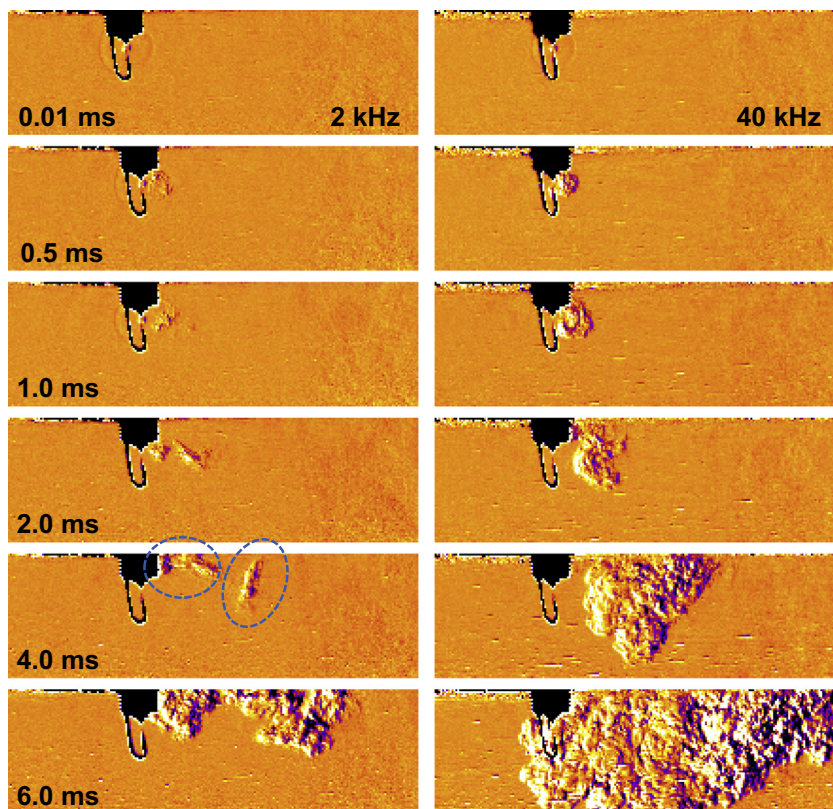
Fig. 4. Ignition kernel development in stoichiometric methane–air mixtures for 5 pulses at 22 kV pulse amplitude (3.2 mJ/pulse). Left images: pulse repetition frequency of 2 kHz. Right images: pulse repetition frequency of 40 kHz.
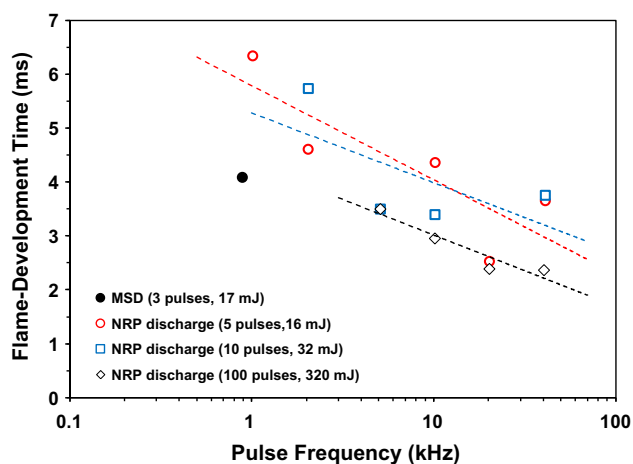
Fig. 5. Flame-development time extracted from schlieren imaging of stoichiometric methane–air ignition for varying frequency at fixed total energy deposition.

which often resulted in quenching of the individual kernels and unsuccessful ignition. The 40 kHz condition is displayed in the right panels. Here, all of the discharge pulses are deposited into a single large ignition kernel since the gas only travels 0.2–0.3 mm between discharge pulses. By the 0.5 ms image, the five pulses have already completed (0.375 ms earlier) and a large single ignition kernel has formed, which is then transported away from the electrode region, where it proceeds to transition into a self-propagating flame and by 6 ms has already expanded into most of the observation domain. Figure 5 shows the trend of decreasing flame-development time with increasing repetition frequency for fixed energy inputs. The three energy conditions show similar

trends of decreasing flame-development time with increasing pulse frequency.

Note that for the same repetition frequency (0.869 kHz) and total energy input ($\approx$16 mJ), the MSD ignition has a shorter flame-development time than the NRP discharge. This can be attributed to the substantial difference of pulse duration between NRP discharges ($\approx$20 ns) and the MSD ($\approx$1 µs), resulting in a higher per pulse energy for the MSD igniter, as summarized in Table 1. At the MSD frequency (0.869 kHz), only one discharge pulse can be deposited into an ignition kernel before it moves away from the electrode region, preventing the inter-pulse coupling effects observed for high-frequency NRP discharges. Thus, for low frequency pulsed discharges, the flame-development time is not a function of the total energy deposition, only the per-pulse energy deposition. The flame-development time of the NRP discharge becomes shorter than that of the MSD at pulse repetition frequencies greater than 5 kHz, indicating the activation of inter-pulse coupling effects. The details of these effects will be discussed in the following sections. Also note that in Figs. 3 and 5 there is significant scatter in the collected data. This is largely due to variations in the flow velocity, which has a particularly large effect when the inter-pulse time is on the same order as the ignition kernel residence time, and thus small flow variations can alter the number of pulses deposited into a single ignition kernel.

To visualize the plasma characteristics in more detail, high-frequency images of NRP discharges in air were taken at a rate of 390 kfps. The plasma emission intensity is plotted for three different pulse frequencies at 22 kV pulse amplitude (3.2 mJ/pulse) in Fig. 6a. The plasma emission is completely quenched between pulses for 5 kHz and 10 kHz pulse repetition frequencies, whereas for 40 kHz repetition frequency the emission is always visible and the minimum emission intensity between the pulses reaches a steady state by the third pulse. In Fig. 6b, the emission intensity
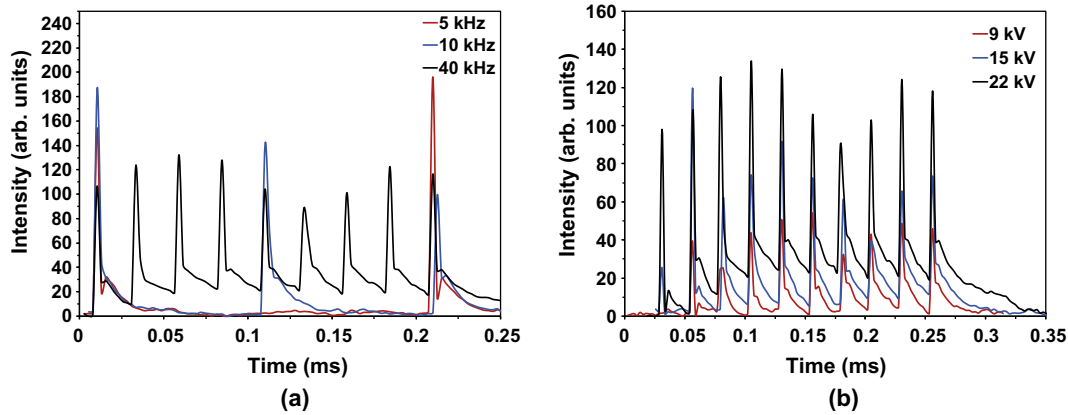
Fig. 6. (a) Plasma emission intensity in air for three different pulse frequencies at 22 kV pulse amplitude (3.2 mJ/pulse). (b) Plasma emission intensity for three different pulse amplitudes at 40 kHz pulse repetition frequency.
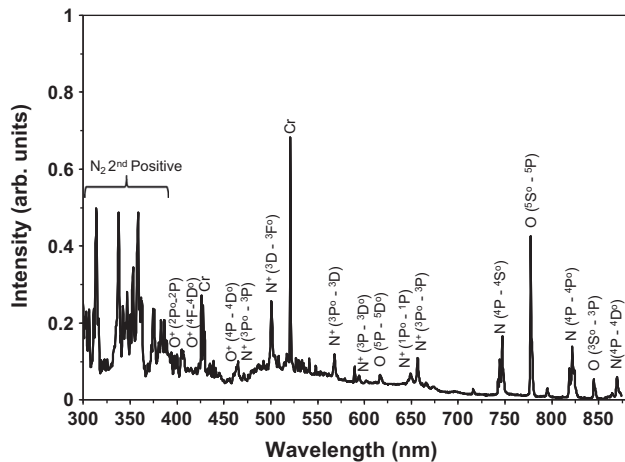
Fig. 7. Emission spectrum in air from a burst of 50 pulses at 22 kV pulse amplitude (3.2 mJ/pulse) and 40 kHz repetition frequency.

at three different pulse amplitudes and 40 kHz pulse repetition frequency is presented. At 9 kV pulse amplitude, little residual emission builds up between pulses, while for 15 kV pulse amplitude the minimum emission between pulses is continuously building up, and for 22 kV pulse amplitude the minimum emission again rapidly builds up to a steady state. These images indicate that active species remain in the inter-electrode region long after the voltage pulse has ended, and their concentration is large enough to effect subsequent pulses in the burst. To identify the species contributing to the emission, OES measurements were conducted, also in air. The results are presented in Fig. 7 for a burst of 50 pulses at 40 kHz repetition frequency and 22 kV pulse amplitude, which represent the highest energy discharge used for this study. The emission lines were compared with the NIST atomic spectral database [40] and the lines tabulated in Ref. [41]. Clearly visible are lines from the N_2 2nd positive system ($C^3\Pi_u \rightarrow B^3\Pi_g$) in the 300–400 nm range, O^+ and N^+ ions in the 400–700 nm range, and O and N atoms in the 700–900 nm range. There are also two strong Cr lines at 426 nm and 521 nm from the stainless steel ground electrode, and below 300 nm there are strong lines from other metal ions, including Fe, Cu, and Ni (not shown). The emission lines are in good agreement with the OES measurements of Pancheshnyi et al. [17] in air under similar conditions. Thus, the discharge is a source of radicals, ions, and excited species, and for sufficiently high pulse frequency and peak amplitude, this source can continuously supply active species to the ignition kernel. The emission

images explain why the high voltage cases (15 kV and 22 kV) are more effective than the low voltage case (9 kV), and also why increasing frequencies continually decrease the flame-development time. The maintenance of a constant radical pool in the center of the ignition kernel is the critical factor in decreasing the flame-development time for multiple pulse ignition devices.

To fully connect the observation of a constant radical pool formed by the plasma to the decrease in flame-development time, the concept of critical radius can be utilized. The process of kernel development from an ignition energy source to a self-propagating flame has been investigated both theoretically [5,42,43] and experimentally [3,9,42] for laminar flames. The development process can be divided into three regimes: spark assisted ignition kernel propagation (Regime I), unsteady transition from spark ignition to laminar flame propagation (Regime II), and laminar flame propagation (Regime III). The first two regimes are sensitive to the initial energy addition, while the final regime is only a function of fuel chemistry. Increased energy addition can decrease the time needed to get to the critical radius, but cannot reduce the magnitude of the critical radius, unless the initial ignition volume becomes comparable to the critical radius. At a given initial energy, the time to the critical radius is controlled solely by the induction chemistry of the mixture, thus, to understand the effect of heat and radical addition on flame-development time, we must understand their effect on the induction chemistry. The emission spectrum showed the presence of excited N_2, N, O, N^+, and O^+. After the discharge, these species will react with the surrounding gas and be partially quenched before the next pulse arrives. To help understand this reaction process, particularly for the case when fuel is present, numerical modeling of the plasma and subsequent combustion processes for stoichiometric methane–air was conducted. The model predicts that the main radicals produced in the plasma discharge are O atoms resulting from dissociation of O_2 by electron collision reactions and by quenching reactions with excited N_2, which is in agreement with previous NRP discharge studies, i.e. [23,44]. The dissociation of O_2 is the dominant radical production channel, as opposed to the dissociation of N_2, since O_2 has a bond dissociation energy (BDE) of 119 kcal/mol as compared to the 226 kcal/mol BDE of N_2. The production pathways for O atom formation in and after the plasma are presented in Fig. 8 for a single pulse of 320 Td peak E/N, initial temperature of 850 K, and pressure of 1 atm. The main production reactions of O atoms are:

$$e + O_2 \rightarrow e + O + O \tag{R1}$$

$$N_2(A, B, a', C) + O_2 \rightarrow N_2 + O + O \tag{R2-R5}$$
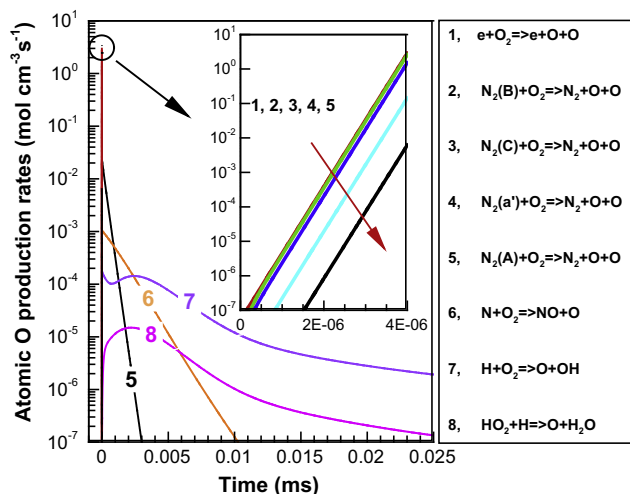
Fig. 8. O atom production rates for a single pulse of 100 ppm of O atom generation in a stoichiometric methane–air mixture at 850 K initial temperature and 1 atm pressure.

$$N + O_2 \rightarrow NO + O \tag{R6}$$

$$H + O_2 \rightarrow O + OH \tag{R7}$$

$$HO_2 + H \rightarrow O + H_2O \tag{R8}$$

The consumption reactions are:

$$CH_4 + O \rightarrow CH_3 + OH \tag{R9}$$

$$CH_3 + O \rightarrow CH_2O + H \tag{R10}$$

$$CH_2O + O \rightarrow HCO + OH \tag{R11}$$

$$HO_2 + O \rightarrow OH + O_2 \tag{R12}$$

During the plasma, the largest formation route is through electron impact dissociative excitation of O_2. The next four major routes are the quenching reactions of the electronically excited states of N_2. After the discharge pulse, quenching of the excited $N_2(A,B,a',C)$ states becomes the dominant pathway until these states are depopulated, which is in accordance with the experimental measurements of Refs. [23,45]. N atoms also produced in the discharge will react with O_2 in (R6) until the N atoms are consumed. At this point the typical combustion reactions (R7) and (R8) take over as the dominant radical production processes. For all of the conditions simulated in this work, reactions (R1)–(R5) were responsible for at least 70% of O atom production, while (R7) and (R8) reactions never accounted for more than 20%, even when the mixture was close to ignition. Consumption of O atoms is through reaction with the fuel and fuel intermediates, with a negligible amount recombining into O_2. Based on the model results, the main effect of the plasma is to produce active species, which quench to produce O atoms and release heat. The O atoms go on to initiate the fuel oxidation process, which results in chain propagating and branching reactions which maintain the population of O atoms and other radicals until the next pulse arrives. We will now numerically investigate how the plasma produced O atoms and heat release contributes to the observed inter-pulse coupling effects.

First we explore the effect of varying pulse repetition frequency. In Fig. 9a, pulses each producing 150 ppm of O atoms are applied at three different pulse repetition frequencies. Similar to the emission intensity measurements from Fig. 6a, increased pulse frequencies result in higher concentrations of O atoms in the inter-pulse

region, and also an accumulation of O atoms in the 40 kHz case. Joule heating by the plasma, as well as quenching of active species and extraction of chemical enthalpy from the fuel incrementally increases the temperature of the mixture after each pulse. This in turn accelerates the rate of fuel oxidation by O atoms (R9)–(R11), which results in the activation of chain branching reactions, particularly (R7). Thus, a coupled cycle of heat and radical production in the plasma, subsequent fuel oxidation, further generation of radicals in the combustion process, and then another pulse to restart the cycle at an increased temperature is set up in the repetitively pulsed system. This numerical experiment demonstrates that the timescale of the radical consumption reactions is long enough for repetitive pulses to build up and sustain a radical pool, provided the temperature is sufficiently high so that chain branching chemistry can occur.

Figure 9b presents the effect of different degrees of O atom generation (Case I: 50 ppm, Case II: 100 ppm, Case II: 150 ppm) at a fixed pulse frequency of 40 kHz. Similar to Fig. 6b, the O atom concentration and temperature in Cases II and III builds up throughout the pulse burst, while there is negligible build up of O atoms for Case I since the consumption reactions are fast enough to return the O atom concentration back to the original value, and the temperature is not high enough for chain branching combustion reactions to increase the radical concentration. Higher pulse energy allows for greater increases in temperature, driving faster fuel oxidation reactions, more radical generation in the combustion process, and thus stronger pulse-to-pulse coupling. In the actual spark discharge, the radicals and heat produced in the narrow discharge region will quickly diffuse outwards from the discharge center, setting up a radical gradient on the border of the discharge region where reaction with the unburned fuel–air mixture begins to occur. The larger the radical pool in the discharge center, the greater the radical flux to the unburned mixture, and thus the faster the flame-development process will proceed. The flame-development time is then sensitive to how quickly a flame can be formed in this radical/temperature gradient, which is a function of the induction chemistry of the particular fuel. Similar numerical predictions performed by Do et al. [46] modeled hydrogen–air ignition using NRP discharges, and also found that the temperature and radical pool build up is a function of pulse frequency and pulse energy. It was found that high frequency and low pulse energy discharges were more effective than low frequency and high pulse energy discharges (using the same overall power deposition) only if the radical consumption rates were faster than production rates, which was true up to 800 K. In the case of methane–air, radical consumption is faster than production even up to 1300 K, as shown in Fig. 9, due to the significantly slower rates of chain branching reactions in methane compared to hydrogen. Following this result, investigation of the differences in induction chemistry between methane and ethylene will lend insight as to why there is a significant reduction in flame-development time for stoichiometric methane–air, but not for ethylene–air.

Pancheshnyi et al. [17] observed that repetitive pulses only had a strong effect on ignition time for mixtures with MIE larger than the individual pulse energy. Stoichiometric ethylene–air has an MIE of 0.096 mJ, which is a factor of five smaller than the 0.49 mJ MIE of stoichiometric methane–air [47]. The MIE increases with flow velocity and turbulent intensity [6,7], thus, it is reasonable to consider methane–air mixtures in the present experiments to have a comparable MIE to the individual pulse energy of the plasma, especially for the 0.8 mJ/pulse condition, while the ethylene–air MIE is less than the individual pulse energy. As mentioned earlier, the critical radius is a useful parameter for describing the ignition kernel to self-propagating flame dynamics. Calculations to find the critical flame radius for stoichiometric methane–air and ethylene–air mixtures were performed using the Adaptive
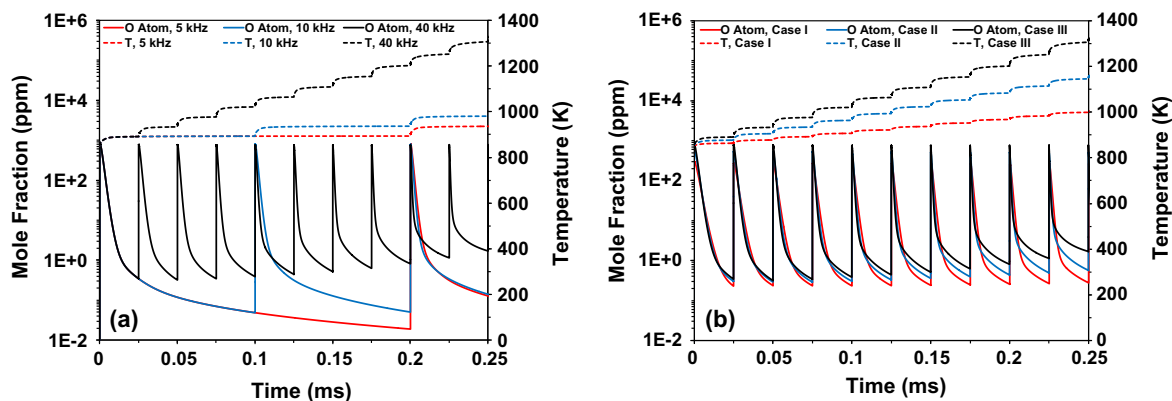
Fig. 9. Computed atomic oxygen concentration and temperature as a function of time for stoichiometric methane–air mixtures at 850 K initial temperature and 1 atm pressure with (a) 150 ppm O atom production repeated at 5 kHz, 10 kHz, and 40 kHz frequencies, and (b) with 50 ppm (Case I), 100 ppm (Case II), and 150 ppm (Case III) O atom production repeated at 40 kHz frequency.

Simulation of Unsteady Reacting Flow (A-SURF) [42] code, again using USC-Mech II [39] for the combustion model. The critical radii were found to be 0.573 cm and 0.462 cm for methane–air and ethylene–air, respectively. Indeed, MIE can be correlated to the cube of the critical radius [5]. Although the computed critical radii for both mixtures are comparable, MIE for ethylene is estimated to be less than 52% of that methane, which is qualitatively consistent to the measured MIE discussed above. However, it is also important to consider the time to reach the critical radius for both mixtures, which is very sensitive to the induction chemistry of the mixture. The methane–air mixture took 2.34 ms to reach to critical radius, while the ethylene–air mixture took only 0.586 ms, both using the same initial hot spot temperature of 1600 K and radius of 2 mm. This result indicates that the induction chemistry time scale is significantly different for the two fuels.

Once again extending the analogy of ignition delays in homogenous mixtures, Fig. 10 shows the ignition delay time for one pulse and five pulses of plasma, each generating 100 ppm of O atoms repeated at 40 kHz, for both ethylene–air and methane–air stoichiometric mixtures. The ignition delay for methane–air is two orders of magnitude longer than for ethylene–air with one pulse, and is as much as three orders of magnitude longer for five pulses. For both fuels, increasing the pulse number from one to five results
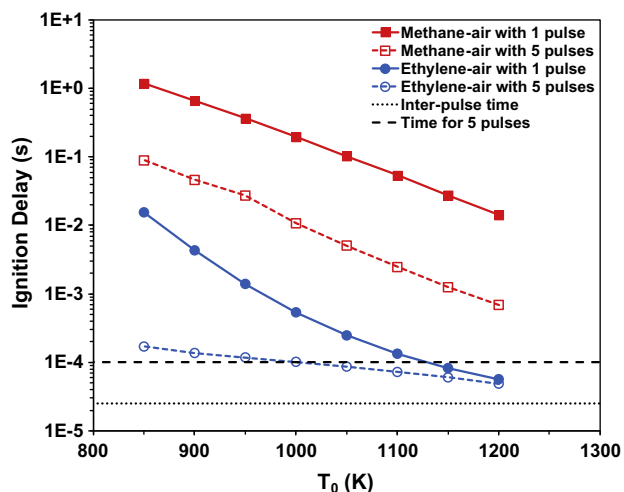
in a decrease in the ignition delay, however, the absolute time reduction for methane–air is two orders of magnitude greater than for ethylene–air. Because the induction chemistry of ethylene is so fast with just a single pulse, the effect of additional pulses is not noticeable on the time scale of the present experiments. In addition, note that the ignition delay of ethylene air for 1 pulse and 5 pulses converge at temperatures above 1000 K. This is due to the ignition delay time approaching the inter-pulse time, resulting in discharge pulses being deposited after ignition has commenced in the 5 pulse case. Do et al. [46] found a similar convergence between autoignition and plasma-assisted ignition for hydrogen–air at temperatures above 1200 K. This illustrates the competition between heat and radical generation from chemical chain branching reactions or from the plasma discharge. If the induction chemistry produces heat and radicals faster than the plasma discharge, no reduction in the ignition delay can be observed by depositing additional energy. From the standpoint of ignition enhancement, it is far more beneficial to apply multiple discharge pulses to a mixture with a long ignition delay time, i.e. large MIE, as compared to a fuel which is easily ignited and thus can only be marginally improved.

3.2. PDE testing

The flow visualization experiments demonstrated that the flame-development time could be reduced using NRP discharges as an ignition source. This section demonstrates the usefulness of this result in a pulsed detonation engine. The thrust output of a PDE is dependent on the frequency of detonation tube usage, which is limited by how quickly each tube can be ignited, transition to a detonation, and exhaust the burned gas to produce thrust. Within this cycle, the ignition process typically consumes the longest period of time, and is thus the limiting process determining the firing frequency of each tube [16]. For a PDE, there are two basic methods to successfully produce a detonation wave: direct initiation or indirect initiation. Direct initiation requires an ignition source with enough energy to produce a strong shock wave that directly produces a coupled auto-ignition wave. The amount of energy required for direct initiation is beyond the capability of practical ignition systems. Indirect ignition occurs when a turbulent deflagration wave is formed in a confined volume such that sufficient heat release is produced to thermally choke the flow, which results in subsequent pressure wave and ignition coupling and leads to detonation. The detonation velocity is solely a property of the gas mixture, so the only opportunity to decrease the duration of the firing phase of the PDE cycle is by decreasing the ignition time and DDT time. Thus, PDEs are an ideal platform to

Fig. 10. Computed ignition delay time as a function of initial temperature for stoichiometric methane–air and ethylene–air mixtures with 1 pulse and 5 pulses of 100 ppm O atom production per pulse repeated at 40 kHz and at 1 atm pressure.
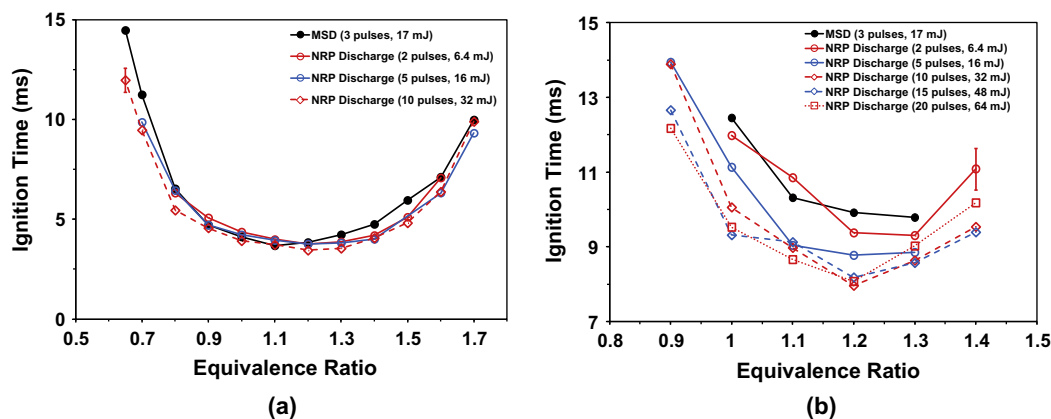
Fig. 11. Ignition time in a PDE as a function of equivalence ratio for MSD ignition and NRP discharges at 22 kV pulse amplitude (3.2 mJ/pulse), 40 kHz repetition frequency. (a) Ethylene–air mixtures and (b) avgas–air mixtures.
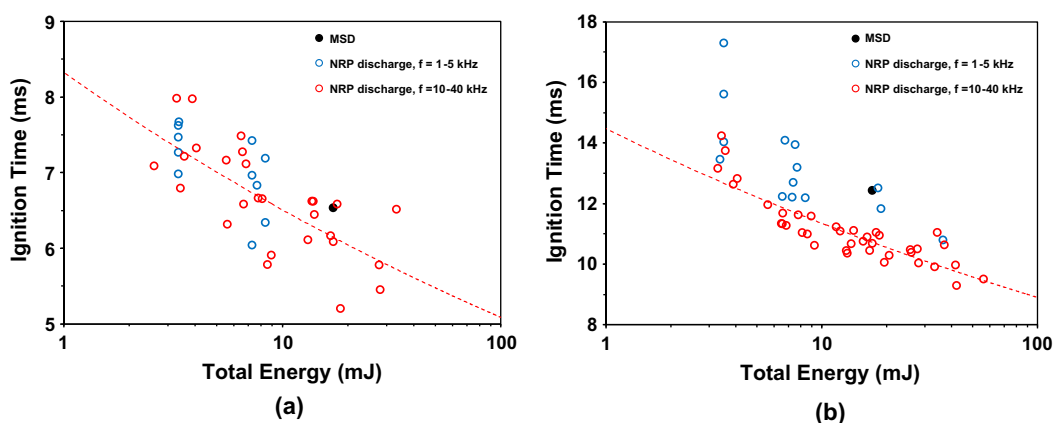
Fig. 12. Ignition time in PDE engine as a function of total energy deposition. (a) Ethylene/air, $\varphi = 0.8$. (b) Avgas–air, $\varphi = 1.0$.

test new ignition methods in an application in which the flame-development time is the limiting factor.

The effects of pulse frequency, pulse amplitude, and pulse number on PDE ignition time were studied by varying each of these parameters independently in two different fuels and a wide range of equivalence ratios. Each condition was run for five ignition events and the plotted data is the average of these data points. The discharge characteristics used for testing are listed in Table 1. For all of the conditions tested, the ignition method had no effect on the DDT distance or time (measured independent of the ignition time). Thus, all of the results presented below focus on the ignition time (analogous to the flame-development time in the flow visualization study) as measured by the pressure rise at the engine head.

To quantify the maximum reduction in ignition time for varying equivalence ratios, the NRP power supply was held constant at its peak pulse amplitude (22 kV) and peak repetition frequency (40 kHz) while the number of pulses was varied from 2 to 20 for avgas–air and 2 to 10 for ethylene–air mixtures for a range of equivalence ratios. The ignition times as a function of equivalence ratio for ethylene–air and avgas–air mixtures are plotted in Fig. 11. For ethylene–air mixtures, there are negligible differences in ignition time between the NRP discharge and MSD, exhibiting only slightly shorter ignition times using the NRP discharge for very lean mixtures ($\varphi \leqslant 0.8$). However, for avgas–air, the ignition time is found to be significantly reduced by the NRP discharge when more than two pulses are applied. This pronounced reduction of ignition time for avgas–air over ethylene–air mixtures can be

explained by the significant difference of MIE between the two tested fuels, as discussed in the previous section. By assuming iso-octane as an avgas surrogate, the MIE of a stoichiometric mixture is estimated to be 1.35 mJ [47]. This is more than a factor of two greater than stoichiometric methane–air, and more than an order of magnitude greater than stoichiometric ethylene–air. Consequently, the ignition time of stoichiometric avgas–air can be reduced by up to 25% using NRP ignition as compared to MSD ignition. Near the lean and rich limits, the MIE increases dramatically [48], thus, the 10–20 pulse NRP discharge most significantly reduces ignition time in these regions. For avgas–air, the NRP discharge could also extend the lean limit to an equivalence ratio of 0.9 and the rich limit to 1.4, representing a 0.1 improvement in equivalence ratio at both extremes.

To explore the effects of specific discharge characteristics, the equivalence ratio for both ethylene–air and avgas–air mixtures were held constant while the plasma parameters were varied. For ethylene–air, $\varphi = 0.8$ was selected; while for avgas–air, $\varphi = 1.0$ was selected, as these equivalence ratios represent cases in which the NRP discharge produced significantly shorter ignition times compared to the MSD discharge, while both systems regularly achieved successful ignition and DDT. The plasma frequency, pulse amplitude, and number of pulses were varied individually. The results of these tests are plotted in Fig. 12. Similar to the flow visualization experiments, two trends emerged in the data. The first is the decrease in ignition time with increase in total energy, as illustrated by the best fit trend line to the 10–40 kHz data. The number of pulses and pulse amplitude, when varied

independently, had similar effects on ignition time, provided the pulses were applied within a time scale much shorter than the overall ignition time. The second trend observed is the decrease of ignition time with increased pulse frequency, even at fixed total energy deposition. This trend is significantly more apparent in the avgas–air data, in which all of the ignition times using less than 10 kHz pulse repetition frequency are above the average of the 10–40 kHz data. Thus, the same results from the flow visualization study are attainable in PDE engine conditions.

4. Conclusions

The effect of nanosecond repetitively pulsed plasma discharges on ignition has been studied in both flame-development visualization and PDE testing platforms. Clear decreases in the visual flame-development time and PDE ignition time were observed for the NRP discharge as compared to conventional spark ignition for a variety of fuels, equivalence ratios, and discharge parameters. In addition, both leaner and richer ignition could be achieved for avgas–air mixtures in the PDE experiments as compared to MSD ignition. The experimental observations are: (1) reduction in flame-development time (or ignition time in the PDE) using NRP discharges was observed only for methane–air and avgas–air mixtures, indicating that a significant impact can be achieved for fuels with slow induction chemistry; (2) flame-development time is decreased as the total ignition energy is increased beyond the mixture's MIE, either by higher pulse amplitudes or by increased pulse number; (3) high frequency pulses (in this case 10–40 kHz) allow the opportunity for multiple pulses to be coupled into an enlarged single flame kernel, resulting in a shorter flame-development time compared to the formation of individual non-interacting flame kernels at lower frequencies; and (4) high frequency (>10 kHz) and high pulse amplitude (>9 kV) discharges in air generate excited and ionized species in the inter-electrode region, the reaction timescales of which are longer than the inter-pulse time. Therefore, inter-pulse coupling between subsequent plasma pulses is an important mechanism to enhance ignition due to an increase in the kernel radical pool and temperature, and thus a reduction in the induction chemistry timescale.

Numerical modeling of homogenous fuel–air mixtures revealed O atoms as the active species with the highest concentration generated by the plasma discharge, which are mainly generated by electron collision reactions with O_2 and quenching of $N_2(A,B,a',C)$ by O_2. The main consumption pathway for O atoms is via reaction with the fuel and its primary intermediates. In addition, heat is generated in and after each discharge pulse, increasing the rate of O atom reaction with the fuel and chain branching reactions in the combustion process. Thus, a positive feedback loop is established by the NRP discharge, consisting of: (1) heat and active species production during the plasma discharge; (2) production of O atoms via quenching reactions just after the discharge; (3) initiation of fuel oxidation by O atom reactions with the fuel and its primary intermediates; (4) radical chain branching reactions sustaining or building the radical pool during the inter-pulse time; and (5) further building of the radical pool and gas temperature by subsequent discharge pulses. This positive feedback loop was particularly effective for high pulse frequencies and pulse amplitudes, in which the minimum O atom concentration could be continually increased during the inter-pulse time for every subsequent discharge pulse. This inter-pulse coupling resulted in more than an order of magnitude decrease in the computed ignition delay going from one pulse to five pulses at 40 kHz repetition frequency and 100 ppm O atom generation per pulse.

Additionally, it was shown that the induction chemistry of fuels with high MIEs, which correspond to large critical radii and long induction chemistry timescales, are much more sensitive to increased energy deposition than are fuels with smaller MIEs. Accordingly, methane–air mixtures exhibited significantly greater decreases in the flame-development time as compared to ethylene–air mixtures subjected to the same degree of plasma energy deposition during the flame-development visualization experiments. This result was also observed in the PDE testing experiments, in which NRP discharge ignition improved ignition time for stoichiometric avgas–air mixtures by 25%, and increased the equivalence ratio range by 50%, as compared to MSD ignition. However, there was only a slight improvement in the ignition time of ethylene–air mixtures, and no expansion of the equivalence ratio operating limits. Based on the observations in these experiments, further improvement in flame-development times can be achieved by using NRP plasma discharges with greater pulse repetition frequency, which would increase the buildup of excited species in the flame kernel and allow more pulses to be applied before the flame front leaves the inter-electrode region.

Acknowledgments

References

[1] Y. Ju, W. Sun, Prog. Energy Combust. Sci. 48 (2015) 21–83.
[2] A. Starikovskiy, N. Aleksandrov, Prog. Energy Combust. Sci. 39 (1) (2013) 61–110.
[3] R. Maly, in: J.C. Hilliard, G.S. Springer (Eds.), Fuel Economy in Road Vehicles Powered by Spark Ignition Engines, Plenum Press, New York, NY, 1984, pp. 91–148.
[4] J.B. Heywood, Internal Combustion Engine Fundamentals, McGraw-Hill, 1988.
[5] Z. Chen, M.P. Burke, Y. Ju, Proc. Combust. Inst. 33 (1) (2011) 1219–1226.
[6] D.R. Ballal, A.H. Lefebvre, Symp. (Int.) Combust. 15 (1) (1975) 1473–1481.
[7] M.-W. Peng, S. Shy, Y.-W. Shiu, C.-C. Liu, Combust. Flame 160 (9) (2013) 1755–1766.
[8] Y.P. Raizer, Gas Discharge Physics, Springer-Verlag, Berlin, 1991.
[9] H.H. Kim, S.H. Won, J. Santner, Z. Chen, Y. Ju, Proc. Combust. Inst. 34 (1) (2013) 929–936.
[10] S.M. Starikovskaia, J. Phys. D: Appl. Phys. 39 (16) (2006) R265–R299.
[11] A.Y. Starikovskii, N.B. Anikin, I.N. Kosarev, E.I. Mintoussov, S.M. Starikovskaia, V.P. Zhukov, Pure Appl. Chem. 78 (6) (2006) 1265–1298.
[12] F. Wang, J.B. Liu, J. Sinibaldi, C. Brophy, A. Kuthi, C. Jiang, P. Ronney, M.A. Gundersen, IEEE Trans. Plasma Sci. 33 (2) (2005) 844–849.
[13] T. Shiraishi, T. Urushihara, M. Gundersen, J. Phys. D: Appl. Phys. 42 (13) (2009) 135208.
[14] C. Cathey, J. Cain, H. Wang, M.A. Gundersen, C. Carter, M. Ryan, Combust. Flame 154 (4) (2008) 715–727.
[15] D. Singleton, S.J. Pendleton, M.A. Gundersen, J. Phys. D: Appl. Phys. 44 (2) (2011) 022001.
[16] K. Busby, J. Corrigan, S.-T. Yu, S. Williams, C. Carter, F. Schauer, J. Hoke, C. Cathey, M. Gundersen, in: 45th AIAA Aerospace Sciences Meeting, Reno, NV, 2007.
[17] S.V. Pancheshnyi, D.A. Lacoste, A. Bourdon, C.O. Laux, IEEE Trans. Plasma Sci. 34 (6) (2006) 2478–2487.
[18] V.P. Zhukov, A.E. Rakitin, A.Y. Starikovskii, J. Propul. Power 24 (1) (2008) 88–93.
[19] A.E. Rakitin, A.Y. Starikovskii, Combust. Flame 155 (1–2) (2008) 343–355.
[20] A. Starikovskiy, N. Aleksandrov, A. Rakitin, Phil. Trans. R. Soc. A 370 (1960) (2012) 740–773.
[21] D.Z. Pai, D.A. Lacoste, C.O. Laux, J. Appl. Phys. 107 (9) (2010) 093303.
[22] D.Z. Pai, D.A. Lacoste, C.O. Laux, Plasma Sour. Sci. Technol. 19 (6) (2010) 065015.
[23] D.L. Rusterholtz, D.A. Lacoste, G.D. Stancu, D.Z. Pai, C.O. Laux, J. Phys. D: Appl. Phys. 46 (46) (2013) 464010.
[24] F.R. Schauer, J.S. Stutrud, R.P. Bradley, in: 39th AIAA Aerospace Sciences Meeting, Reno, NV, 2001.
[25] K.C. Tucker, P.I. King, F.R. Schauer, J. Propul. Power 24 (4) (2008) 788–796.

[26] C. Stevens, V. Gamezo, P. King, F. Schauer, J. Hoke, in: 49th AIAA Aerospace Sciences Meeting including the New Horizons Forum and Aerospace Exposition, Orlanda, FL, 2011.
[27] J. Canny, IEEE Trans. Pattern Anal. 6 (1986) 679–698.
[28] J. Santner, F.L. Dryer, Y. Ju, Proc. Combust. Inst. 34 (1) (2013) 719–726.
[29] S. Pancheshnyi, B. Eismann, G.J.M. Hagelaar, L.C. Pitchford, University of Toulouse, LAPLACE, CNRS-UPS-INP, Toulouse, France, 2008. <http://www.zdplaskin.laplace.univ-tlse.fr>.
[30] G.J.M. Hagelaar, L.C. Pitchford, Plasma Sour. Sci. Technol. 14 (4) (2005) 722–733.
[31] A.E. Lutz, R.J. Kee, J.A. Miller, Sandia National Laboratories Report SAND87-8248, 1988.
[32] A. Flitti, S. Pancheshnyi, Eur. Phys. J.-Appl. Phys. 45 (2) (2009) 21001.
[33] N.L. Aleksandrov, S.V. Kindysheva, E.N. Kukaev, S.M. Starikovskaya, A.Y. Starikovskii, Plasma Phys. Rep. 35 (10) (2009) 867–882.
[34] J.K. Lefkowitz, M. Uddi, B.C. Windom, G. Lou, Y. Ju, Proc. Combust. Inst. 35 (3) (2015) 3505–3512.
[35] Hayashi Database. <www.lxcat.net> (retrieved 04.10.14).
[36] Phelps Database. <www.lxcat.net> (retrieved 04.10.14).
[37] TRINITI Database. <www.lxcat.net> (retrieved 04.10.14).
[38] R.K. Janev, D. Reiter, Phys. Plasmas 11 (2) (2004) 780.
[39] H. Wang, X. You, A.V. Joshi, S.G. Davis, A. Laskin, F. Egolfopoulos, C.K. Law. <http://ignis.usc.edu/USC_Mech_II.htm>.
[40] A. Kramida, Yu. Ralchenko, J. Reader, NIST ASD Team, NIST Atomic Spectra Database (version 5.2), National Institute of Standards and Technology, Gaithersburg, MD, 2014. <http://physics.nist.gov/asd>.
[41] R.W.B. Pearse, A.G. Gaydon, The Identification of Molecular Spectra, 3rd ed., Chapman & Hall, London, UK, 1965.
[42] Z. Chen, Studies on the Initiation, Propagation, and Extinction of Premixed Flames, Princeton University, Princeton, NJ, 2009.
[43] Z. Chen, Y. Ju, Combust. Theory Model. 11 (3) (2007) 427–453.
[44] N.A. Popov, J. Phys. D: Appl. Phys. 44 (28) (2011) 285201.
[45] G.D. Stancu, F. Kaddouri, D.A. Lacoste, C.O. Laux, J. Phys. D: Appl. Phys. 43 (12) (2010) 124002.
[46] H. Do, M.A. Cappelli, M.G. Mungal, Combust. Flame 157 (9) (2010) 1783–1794.
[47] J.B. Fenn, Ind. Eng. Chem. 43 (12) (1951) 2865–2869.
[48] R.A. Yetter, I. Glassman, Combustion, Elsevier, Inc., 2008.